

## HIGH SPECTRAL RESOLUTION OBSERVATIONS OF THE H<sub>2</sub> 2.12 MICRON LINE IN HERBIG-HARO OBJECTS<sup>1</sup>

HANS ZINNECKER

Max-Planck-Institut für Physik und Astrophysik, Institut für Extraterrestrische Physik, Garching

REINHARD MUNDT

Max-Planck-Institut für Astronomie, Heidelberg

T. R. GEBALLE

Joint Astronomy Centre, Hilo

AND

WILLIAM J. ZEALEY

Physics Department, University of Wollongong

Received 1988 July 14; accepted 1988 December 3

### ABSTRACT

We have used the UKIRT infrared Fabry-Perot system to obtain high spectral resolution H<sub>2</sub> 2.12 μm line profiles (resolution = 30–35 km s<sup>-1</sup>) for a number of Herbig-Haro objects. Objects observed include HH 1/2, HH 7–11, HH 19, HH 32A, HH 40, and HH 43B; all are associated with jetlike features of collimated optical outflows. In most cases the velocity structure in the H<sub>2</sub> line resembles that of the higher excitation optical lines (e.g., Hα), but the FWHM and the maximum velocities of the H<sub>2</sub> lines are significantly smaller (by about a factor of 2). We conclude that for the observed objects the following two mechanisms seem to be most important for the H<sub>2</sub> emission: (1) shock heating of external molecular gas in the wings of the bow shock associated with the working surface of a high-velocity jet; and (2) shock heating of external molecular gas entrained in the flow by internal shocks occurring in the jet itself and/or in its boundary layer. The first mechanism is of course only relevant for Herbig-Haro objects associated with the jet's end (e.g., HH 1 or HH 32A), while the second one applies only to Herbig-Haro objects observed along the flow axis (e.g., HH 40 or HH 7–11).

*Subject headings:* infrared: spectra — nebulae: general — shock waves — stars: pre-main-sequence

### I. INTRODUCTION

A large and growing body of observational material indicates that energetic, often bipolar, mass outflows are an important phase in the early stellar evolution of all types of young stars (see, e.g., the reviews of Lada 1985 and Mundt 1985a). Besides the “high-velocity” (10–30 km s<sup>-1</sup>) CO line emission, a major probe of the outflows from young stars are Herbig-Haro (HH) objects. Their optical line emission originates in the cooling regions of high-velocity (40–100 km s<sup>-1</sup>) shock waves. Optical proper motion and radial velocity measurements of HH objects have demonstrated that high-velocity material (200–400 km s<sup>-1</sup>) can be channeled into highly collimated bipolar flows (Herbig and Jones 1981; Graham and Elias 1983; Mundt, Stocke, and Stockman 1983). In several cases the high collimation is directly evident from narrow high-velocity jets extending away from T Tauri stars or from optically obscured infrared sources of comparable luminosity (Mundt and Fried 1983; Mundt *et al.* 1984; Reipurth *et al.* 1986; for a recent review see Mundt 1988). The close physical association and similar optical spectra indicate that these jets and the HH objects are closely related phenomena; e.g., many cataloged HH objects are the brightest knots in these jets, much like the radio hot spots in extragalactic jets of radio galaxies.

In the last few years a number of HH objects have been observed to emit the  $v = 1-0 S(1)$  line and the  $Q$ -branch lines of H<sub>2</sub> (at 2.12 μm and 2.4 μm, respectively). Examples include HH

1/2 and HH 40 (Elias 1980), HH 7–11 and HH 32 (Zealey, Williams, and Sandell 1984; Lightfoot and Glencross 1986; Zealey *et al.* 1986), HH 12 (Lane and Bally 1986), HH 19 (Zinnecker *et al.* 1985), and HH 52, HH 53, and HH 54 (Sandell *et al.* 1987). The H<sub>2</sub> observations of HH objects up to 1986 have been reviewed by Mundt (1987), and a survey of H<sub>2</sub> emission in 16 HH objects has recently been carried out by Schwartz, Cohen, and Williams (1987). There appears to be a rough spatial coincidence between optical and infrared line emission. However, most of these observations were made with large apertures (≈10”), and hence it is often not possible to establish the precise degree of spatial coincidence, an important factor in distinguishing between different HH models. Zealey *et al.* (1988, 1989) have recently mapped several of the brighter extended HH objects in the 2.12 μm H<sub>2</sub> line at higher (≈4”) spatial resolution. The new maps show that the infrared H<sub>2</sub> emission does not always coincide with the optical emission (e.g., Hα or [S II]); displacements of a few arcseconds occur in several cases.

The observed line ratios of H<sub>2</sub> show that these lines, like the optical emission lines, are formed behind radiative shock waves (e.g., Elias 1980; Schwartz, Cohen, and Williams 1987). Assuming pure hydrodynamic shocks with no magnetic fields (e.g., Shull and Hollenbach 1978) shock velocities of 10–20 km s<sup>-1</sup> and preshock densities of several 10<sup>4</sup> cm<sup>-3</sup> are derived. For low preshock densities (10<sup>2</sup>–10<sup>3</sup> cm<sup>-3</sup>) and/or for magnetohydrodynamic shocks (Hollenbach and McKee 1980; Draine, Roberge, and Dalgarno 1983), the shock velocities may be as large as 50 km s<sup>-1</sup> before most H<sub>2</sub> is destroyed by

<sup>1</sup> Based on data collected at the United Kingdom Infrared Telescope, Mauna Kea, Hawaii.

dissociation. Although the exact shock parameters are still unclear, there is little doubt that  $\text{H}_2$  emission is a tracer of shocks between about 10 and 40  $\text{km s}^{-1}$ . Thus these shocks have in general (much) lower velocities than those derived from optical emission lines, for which velocities of about 40–100  $\text{km s}^{-1}$  have been estimated (assuming plane parallel shock waves, e.g., Schwartz 1983). For HH 1 and other HH objects, even higher values of up to 200  $\text{km s}^{-1}$  have been derived from optical data assuming line formation in a bow shock (e.g., Hartmann and Raymond 1984). All of this implies that HH objects are probably associated with rather complex shock structures in which shocks exist with velocities ranging over rather large values (10–200  $\text{km s}^{-1}$ ). One interesting question is therefore how the low-velocity shocks, responsible for the  $\text{H}_2$  emission, are driven and how they relate to the higher velocity shocks producing the optical emission. An answer to this question is available for a high-velocity ( $v \approx 100$ –200  $\text{km s}^{-1}$ ) bow shock propagating in the ambient  $\text{H}_2$  gas. In this case the optical lines and the  $\text{H}_2$  line would result from the same shock and the  $\text{H}_2$  lines would form in the wings of the bow shock where the velocity component perpendicular to the shock surface is sufficiently small.

In addition to high spatial resolution observations of the  $\text{H}_2$  emission, high spectral resolution observations are also needed to discriminate between potential models. For example, quiescent ambient  $\text{H}_2$  gas being excited by low-velocity shocks will have quite different velocities than  $\text{H}_2$  gas being entrained in a high-velocity jet and shock-excited in the flow itself. In this paper we present high spectral resolution  $\text{H}_2$  2.12  $\mu\text{m}$  line profiles which, together with other data available on the observed objects, allow us to construct simple models. In § II of this paper we describe the observations, and in § III we describe the observed  $\text{H}_2$  2.12  $\mu\text{m}$  line profiles. The proposed models and their applications to the observed objects are discussed in § IV. Our conclusions are summarized in § V.

## II. OBSERVATIONS

Spectra of the  $\text{H}_2$   $v = 1-0$   $S(1)$  line at 2.122  $\mu\text{m}$  were obtained at the United Kingdom 3.8 m infrared telescope at Mauna Kea on the nights of 1986 November 20–23. The spectrometer was a scanning Fabry-Perot interferometer mounted in front of a solid nitrogen-cooled cryostat. The latter contains a 1.3–2.6  $\mu\text{m}$  circular variable filter (CVF) of resolving power  $\approx 120$  and a single InSb detector. The CVF, which was tuned to 2.12  $\mu\text{m}$ , blocks all but a few of the orders of the Fabry-Perot near the  $S(1)$  line wavelength. Because the atmosphere is transparent near the  $S(1)$  line and because the  $S(1)$  lines in these HH objects are much brighter than the continua or other lines that might be transmitted by the CVF, the resultant spectra should be excellent representations of the actual spectrum near the  $S(1)$  line.

The resolution of the Fabry-Perot in collimated light is 25  $\text{km s}^{-1}$ . However, for most of the present measurements, a circular aperture of 11" diameter was employed in the cryostat; this lowers the resolution to  $\approx 32$   $\text{km s}^{-1}$ . Small drifts in the Fabry-Perot spacing were observed but were largely compensated for with the aid of frequent observations of an argon lamp employed for wavelength calibration (see below). We believe that the resolution of the final spectra is only slightly degraded by this drift and is  $\approx 35$   $\text{km s}^{-1}$ . A few of the spectra were obtained with a 7" diameter beam; for these the final resolution is  $\approx 31$   $\text{km s}^{-1}$ .

The spectra were sampled about every 10  $\text{km s}^{-1}$ . Integra-

tion times ranged from 1 to 3 s per Fabry-Perot setting. Between six and 48 spectra of each object were co-added to produce the final spectra shown here. Chopping directions and amplitudes were chosen to avoid regions of line emission in the reference beam. Wavelength calibration was derived from a line of argon at 2.0992  $\mu\text{m}$  and from the narrow  $v = 1-0$   $S(1)$  line at Orion Peak 2, whose LSR velocity at peak emission was taken to be +13  $\text{km s}^{-1}$  (Nadeau and Geballe 1979). The wavelength calibration of the HH spectra are believed to be accurate to  $\pm 5$   $\text{km s}^{-1}$ .

## III. RESULTS

Figures 1–6 show the  $\text{H}_2$  2.12  $\mu\text{m}$  line profiles of the HH objects we observed. Relative flux is plotted against LSR radial velocity. The integrated fluxes of the  $\text{H}_2$  lines are typically

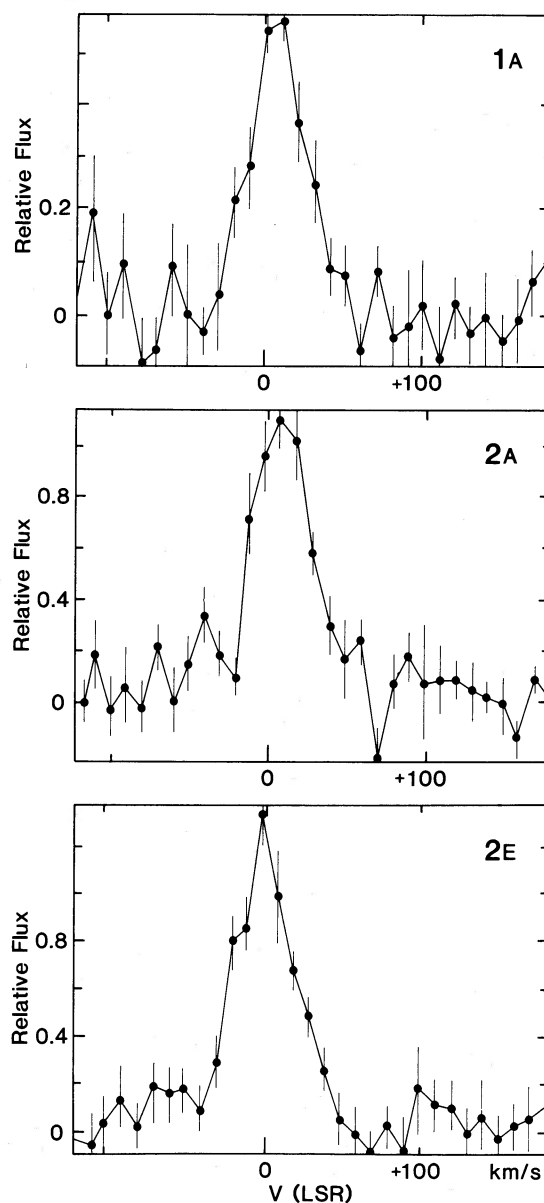
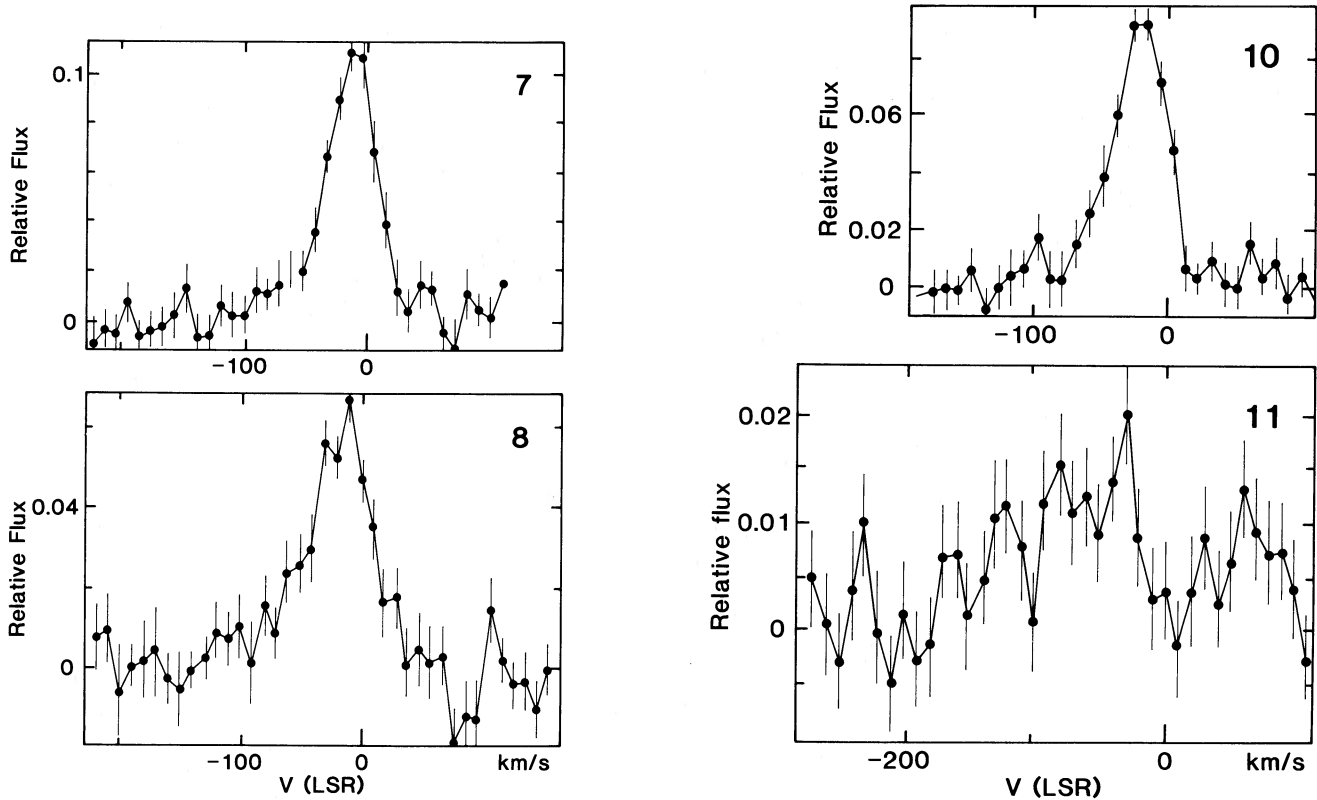


FIG. 1.— $\text{H}_2$  2.12  $\mu\text{m}$  line profile of HH 1A, HH 2A, and HH 2E. The effective spectral resolution in these and the other profiles shown in Figs. 2–6 is 31–35  $\text{km s}^{-1}$ .

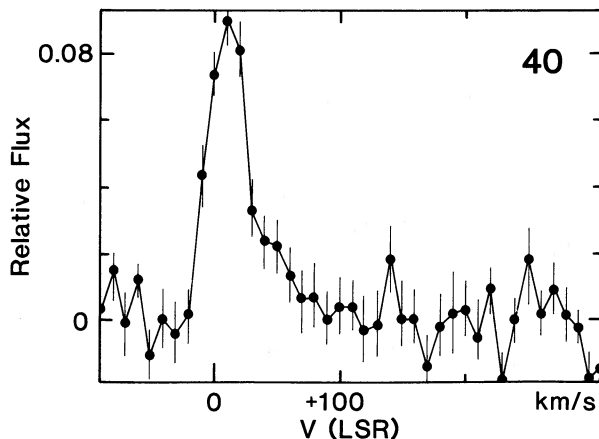
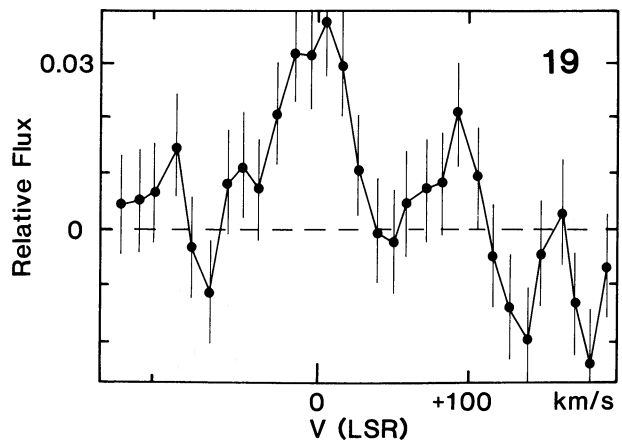
FIG. 2.—H<sub>2</sub> 2.12  $\mu$ m line profile of HH 7, HH 8, HH 10, and HH 11

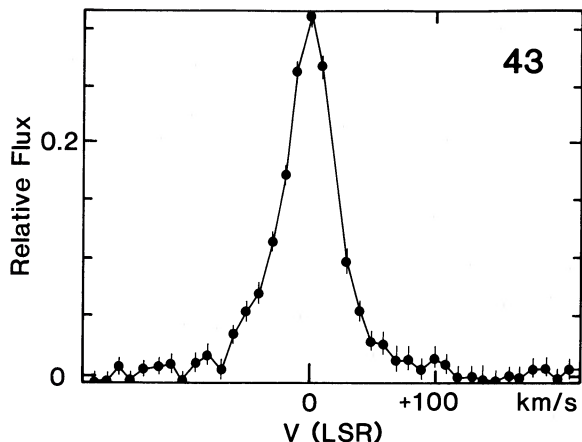
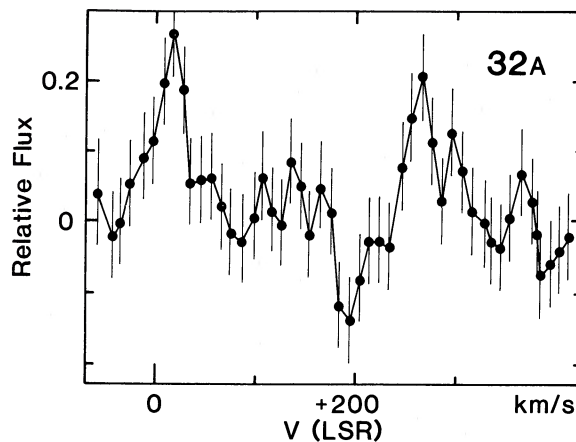
$1-3 \times 10^{-20} \text{ W cm}^{-2}$ , except for HH 43 where the flux is  $\approx 1 \times 10^{-19} \text{ W cm}^{-2}$ . Root mean square error bars are given for each velocity bin. The spectra are not deconvolved, as in most cases the signal-to-noise (S/N) ratios are not sufficiently high for this to produce meaningful results.

Table 1 summarizes the properties ( $V_{\text{peak}}$ , FWHM) derived from the measured  $S(1)$  line profiles and compares them with values derived for the H $\alpha$  line and with the CO data of the ambient molecular cloud. According to the nominal values given in Table 1, most line cores are partially resolved (i.e., FWHM  $> 35 \text{ km s}^{-1}$ ). However, for HH 19 and the high-velocity component of HH 32A the S/N ratio is not high enough to ascertain whether these profiles are indeed resolved.

We regard the line cores of the following six objects as resolved: HH 2A, HH 7, HH 8, HH 10, HH 11, and HH 43B.

The H<sub>2</sub> line profile of HH 40 shows a broad red wing extending to about  $+80 \text{ km s}^{-1}$  (compared to values of about  $+170 \text{ km s}^{-1}$  in the optical; Mundt *et al.* 1984, see their Fig. 4). Similarly, asymmetric H<sub>2</sub> line wings extending to at least  $-70 \text{ km s}^{-1}$  are observed for HH 7, HH 8, and HH 10. As in HH 40, the optical lines in HH 7, HH 8, and HH 10 extend to significantly higher radial velocities ( $\approx -150 \text{ km s}^{-1}$ ; Solf and Böhm 1987, see their Fig. 5). Table 1 shows that much larger widths are normally observed in the optical lines than in the  $S(1)$  line [typically twice as large after correcting the  $S(1)$  line for the instrumental profile]. In HH 32A, two apparently unre-

FIG. 3.—H<sub>2</sub> 2.12  $\mu$ m line profile of HH 40FIG. 4.—H<sub>2</sub> 2.12  $\mu$ m line profile of HH 19

FIG. 5.—H<sub>2</sub> 2.12 μm line profile of HH 43BFIG. 6.—H<sub>2</sub> 2.12 μm line profile of HH 32A

solved velocity components are observed in the  $S(1)$  line (at  $+18 \text{ km s}^{-1}$  and  $+270 \text{ km s}^{-1}$ ). It is remarkable that two components with similar velocities are also observed in the optical (at  $+67 \text{ km s}^{-1}$  and  $+267 \text{ km s}^{-1}$ ). Higher S/N data would be desirable in this case to see whether, like in the optical, there is also H<sub>2</sub> emission between these two components.

HH 1 and HH 2 are the only objects investigated here for which the outflow is very nearly in the plane of the sky, as indicated by the small radial velocity difference between H $\alpha$  and the CO emission of the ambient molecular cloud ( $\leq 14 \text{ km s}^{-1}$ ). Therefore, it is not surprising that the  $S(1)$  line has a velocity similar to that of the CO line. For all other objects the velocity difference between H $\alpha$  and CO is larger than  $40 \text{ km s}^{-1}$ ; for these objects  $V_{\text{peak}}$  of the  $S(1)$  line is shifted with respect to the CO line by at least  $10 \text{ km s}^{-1}$  (except for HH 40, where it is  $8.5 \text{ km s}^{-1}$ ). The shift is always in the same sense as observed in the optical. Note that a shift of  $10 \text{ km s}^{-1}$  seems to be

significant since it is twice as large as the  $1 \sigma$  velocity error of our H<sub>2</sub> measurements.

#### IV. INTERPRETATION AND DISCUSSION

##### a) Justification of the Jet Model

Optical observations of the HH objects studied here have shown that they are all associated with collimated mass outflows or jets from young stellar objects (YSO). References to these optical studies are given in Table 1. This association strongly suggests that the observed HH objects, as in many other cases, represent the brightest radiative shocks in these collimated flows or jets; e.g., internal shocks occurring within the flow itself or near its end in the so-called working surface (Dyson 1984; see also Mundt 1985*b* or Mundt, Brugel, and Bührke 1987 for a detailed justification). This model will be called the jet model and specific cases of it will be discussed below.

TABLE 1

COMPARISON BETWEEN HIGH-RESOLUTION SPECTROSCOPIC OBSERVATIONS OF H $\alpha$  AND FABRY-PEROT H<sub>2</sub>  $S(1)$  OBSERVATIONS

OBJECT	H $\alpha$				H <sub>2</sub> $S(1)$			
	References (jet and collimated flow)	$V_{\text{peak}}$ ( $\text{km s}^{-1}$ )	FWHM ( $\text{km s}^{-1}$ )	FWZI ( $\text{km s}^{-1}$ )	References (velocities)	$V_{\text{peak}}$ ( $\text{km s}^{-1}$ )	FWHM <sup>a</sup> ( $\text{km s}^{-1}$ )	$V(\text{CO})^b$
HH 1A .....	1, 2, 3	-6	50	...	10	+5	38	+8.2
HH 2A .....	1, 2, 3	+7	120	...	11	+7	44	+8.0
HH 2E .....	1, 2, 3	+13	50	...	10	0	40	+8.0
HH 7 .....	4, 5	-51	90	145	12	-4	45	+7.0
HH 8 .....	4, 5	-55	80	125	12	-14	50	+7.0
HH 10 .....	4, 5	-46	50	115	12	-19	50	+7.0
HH 11 .....	4, 5	-179	90	175	12	$\approx -60^c$	110 <sup>c</sup>	+7.0
HH 19 .....	6	-31	25	...	13	-1	50 <sup>c</sup>	+10.0
HH 32A .....	7, 8	+67 <sup>d</sup>	110 <sup>d</sup>	400 <sup>e</sup>	8, 14	+18 <sup>d</sup>	30 <sup>c</sup>	+8.0
		+267 <sup>d</sup>	160 <sup>d</sup>	...	...	+270 <sup>d</sup>	50 <sup>c</sup>	...
HH 40 .....	6	+102	110	200	6, 13	+16	35	+7.5
HH 43B .....	9	-20	$\approx 60$	...	15	-4	45	+6.0

<sup>a</sup> Observed values (not deconvolved).

<sup>b</sup> Velocity of ambient molecular cloud; values from Edwards and Snell 1983.

<sup>c</sup> Poor S/N.

<sup>d</sup> Two components.

<sup>e</sup> Sum for both components.

REFERENCES.—(1) Herbig and Jones 1981; (2) Strom *et al.* 1985; (3) Mundt 1988; (4) Herbig and Jones 1983; (5) Mundt 1985*b*; (6) Mundt *et al.* 1984; (7) Mundt, Stocke, and Stockman 1983; (8) Hartigan, Mundt, and Stocke 1986; (9) Strom *et al.* 1986; (10) Hartmann and Raymond 1984; (11) Böhm and Solf 1985; (12) Solf and Böhm 1987; (13) Mundt, Brugel, and Bührke 1987; (14) Solf, Böhm, and Raga 1986; (15) Böhm and Solf 1989.

Alternative models for HH objects include the shocked cloudlet model (Schwartz and Dopita 1980), the bullet model (Norman and Silk 1979) and the Cantó model (Cantó and Rodríguez 1980). We will not consider the predictions that each of these models makes for the H<sub>2</sub> line emission since none of them appears to apply to the particular HH objects that we have observed. In fact, all of the objects in question show evidence for being associated with jetlike structures visible on deep CCD images. This alignment argues against the shocked cloudlet model, at least in its original form, since the cloudlets would not be expected to be aligned in one direction just by chance. Similarly, the bullet model (although it has certain features in common with the jet model, especially if there is only a single HH knot) would require all the "bullets" to be ejected from the source in two opposite directions, which seems unlikely. We also note that the acceleration of dense clumps in a flow (e.g., a jet) to the full flow speed is probably impossible due to clump destruction (Hartquist and Dyson 1987). This implies that any collimated bipolar flow will very probably not contain high-velocity "bullets." Finally, the Cantó model, at least in its original form, is a static model, yet we know that the HH knots are moving at high speeds. For these reasons it seems justified not to consider these models for the observed objects and we will therefore concentrate on the jet model and its variants.

#### b) Specific Cases of the Jet Model

We consider the following three cases to be most important for the excitation of H<sub>2</sub> emission by a high-velocity jet (see Fig. 7 for illustrations).

1. *H<sub>2</sub> entrainment.*—In this case the H<sub>2</sub> line emission occurs predominantly in the shear layer (turbulent mixing layer in Fig. 7) between the jet and the external H<sub>2</sub> gas. It could, for example, be excited by oblique internal shocks in the jet/collimated flow. If H<sub>2</sub> is continuously entrained, it should have a smaller radial velocity than the optical emission, since material in the shear layer is not yet fully accelerated to the speed of the jet. Recent high-resolution spectroscopic studies of optical jets suggest that entrainment of external gas does occur (Solf 1987; Meaburn and Dyson 1987; Bührke, Mundt, and Ray 1988).

A very interesting variant of the H<sub>2</sub> entrainment case is the following: if H<sub>2</sub> is (only) entrained very close to the source, it may be subsequently accelerated to the full jet speed, i.e., to the same speed as the H I component. This would mean that the jet would consist of a mixture of H I and H<sub>2</sub> at the same velocity. The H<sub>2</sub> would have to be excited in very oblique internal shocks ( $v_{\text{shock}} \approx 10\text{--}40 \text{ km s}^{-1}$ ) to avoid dissociation. In the optical such jets would show very low excitation (e.g., strong [S II] lines). We note that in this case the optical and H<sub>2</sub> emission need not be formed at the same distance from the jet axis, since the internal shocks can be curved (i.e.,  $v_{\text{shock}}$  varies along the shock surface).

2. *External shocks.*—The optical knots in jets or collimated flows are probably the locations of oblique internal shocks (e.g., Mundt 1985b; Mundt, Brugel, and Bührke 1987). If these shocks are excited via Kelvin-Helmholtz instabilities (e.g., Norman, Smarr, and Winkler 1984; Bührke, Mundt, and Ray 1988), then not only internal shocks but also external shocks moving into the surrounding medium are formed. If the surrounding medium contains H<sub>2</sub>, it will be excited by these shocks, provided their velocities are about  $10\text{--}40 \text{ km s}^{-1}$ . Then, if the surrounding medium is quiescent molecular gas

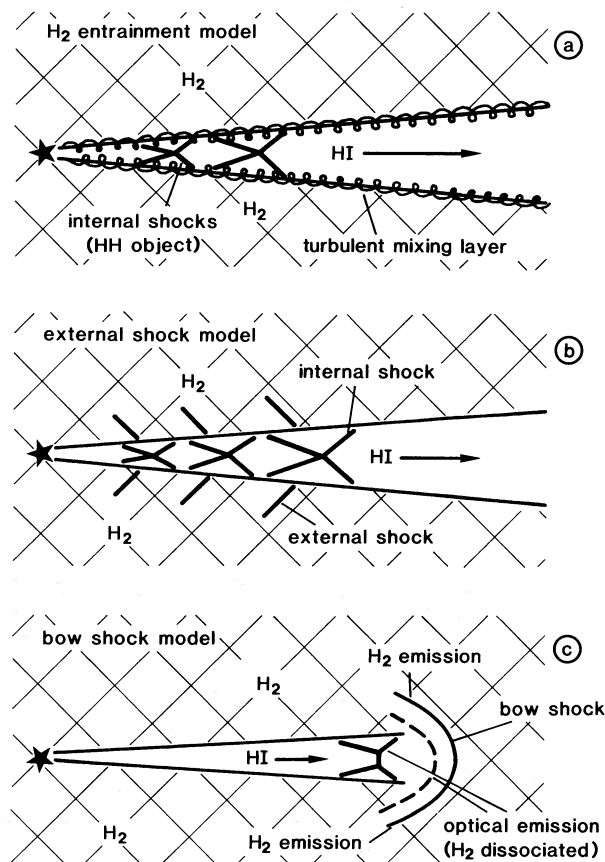


FIG. 7.—H<sub>2</sub> shock excitation models considered here. In all of them a collimated flow or jet interacts with the surrounding molecular cloud.

(i.e., not part of a molecular outflow), the shocked H<sub>2</sub> will have a very small velocity (i.e., approximately the same velocity as the surrounding molecular cloud).

3. *Bow shock.*—A collimated flow or jet will form a bow shock at its end. Optical studies have shown (e.g., Mundt 1986) that the working surface (the region where the jet impacts on the ambient medium) usually propagates with relatively high speeds through the ambient medium ( $\approx 200 \text{ km s}^{-1}$ ). This implies that the external H<sub>2</sub> entering the bow shock will usually be dissociated near its apex and H<sub>2</sub> line emission will therefore predominantly arise in the wings of the bow shock. This H<sub>2</sub> line emission should have small line widths and small radial velocities; i.e., much smaller than the optical emission from the apex region (Raga and Böhm 1986; Hartigan, Raymond, and Hartmann 1987). Obviously this model may only be applicable if H<sub>2</sub> line emission is observed near the working surface.

In principle it is conceivable that the UV photons created in high-velocity shocks associated with the working surface will excite surrounding H<sub>2</sub>. In this case the H<sub>2</sub> line emission should have the same velocity as the surrounding molecular gas and should be concentrated on the brightest optical emission. However, this mechanism does not seem to be very important, since the H<sub>2</sub> line ratios of HH objects indicate shock excitation (Elias 1980; Schwartz, Cohen, and Williams 1987). Furthermore, the UV flux from the working surface appears far too small to account for the observed flux in the H<sub>2</sub> lines (T. W. Hartquist 1988, private communication).

An interesting question is whether  $H_2$  could re-form in the coolest parts of the postshock cooling region ( $T \leq 100$  K), i.e., on dust grains which are expected to survive shock velocities of  $\leq 300$  km s $^{-1}$  (Hollenbach and McKee 1979). According to the rate equation given by Hollenbach, Werner, and Salpeter (1971) it would take about  $3 \times 10^5$  yr to transform most H I into  $H_2$  for an initial H I number density of  $10^4$  cm $^{-3}$ . This is far longer than the typical dynamical time scale of the jets from young stars which is about  $10^3$  yr (Mundt, Brugel, and Bührke 1987) and therefore  $H_2$  reformed behind high-velocity shocks probably does not contribute to the  $H_2$  line emission associated with HH objects. In addition, any line emission from  $H_2$  formed in the postshock cooling region would have similar velocities and velocity dispersion as the optical emission. This is not observed as discussed above in § III.

### c) Discussion of Individual Objects

In the following we will discuss the observed objects on the basis of the above models. It is not obvious in all objects which case of the jet model seems most appropriate. In general, the situation is clearer for those objects where good  $H_2$  maps are available and/or where the flow is sufficiently inclined toward the line of sight; i.e., where high radial velocities are observed in the optical. In this latter case, differences in radial velocity between the  $H_2$  S(1) and optical lines can be measured more easily (see, e.g., HH 40 below).

**HH 1.**—It has been noted by various authors that HH 1 has the shape expected from a radiative bow shock (e.g., Raga *et al.* 1988). The observed  $H_2$  emission peaks on the position of the eastern wing of the bow shock (Harvey *et al.* 1986; Zealey *et al.* 1988, 1989). This, together with the small line width, is fully consistent with the case of a bow shock discussed above. One problem for this interpretation seems to be the fact that  $H_2$  line emission is only observed along one wing. However, in the optical many bow shocks are also nonaxisymmetric (Mundt 1988; Bührke, Mundt, and Ray 1988). Therefore this is not a severe constraint on the interpretation. The other two cases of the jet model very probably do not apply to HH 1 (and to HH 2), since they are mainly relevant to  $H_2$  line emission observed along the flow, as in HH 7–11 or HH 40 (see below).

**HH 2.**—It has been suggested by Raga and Böhm (1987) that HH 2 might result from a bow shock, with the individual condensations (e.g., HH 2A and E) being due to thermal instabilities. In this case the flow and shock pattern in the whole HH 2 region will be rather complex. The observed  $H_2$  S(1) line widths of HH 2A and HH 2E are 40–45 km s $^{-1}$  and are close to our resolution limit of 30–35 km s $^{-1}$ . Thus the true widths are rather small, in the range of 10–25 km s $^{-1}$ , depending on the shape of the intrinsic and instrumental profiles. Such small velocity values are consistent with bow shock theory. By contrast, the FWHM of HH 2A in H $\alpha$  is 120 km s $^{-1}$ . Furthermore the  $H_2$  line emission peaks 5" southwest of knot HH 2A (Harvey *et al.* 1986; Zealey *et al.* 1988, 1989). The extent to which these data can be explained by a high-velocity bow shock with thermal instabilities is unclear. Perhaps strong deviations from axial symmetry are involved, as indicated for other bow shocks (see above).

**HH 7–11.**—The peak of the S(1) line in all four condensations is blueshifted with respect to the surrounding molecular gas. Furthermore the S(1) line profiles of HH 7, 8, and 10 show broad blue wings extending to about  $-70$  km s $^{-1}$  (most clearly for HH 10). For HH 11 broad (FWHM  $\approx 110$  km s $^{-1}$ ) and strongly blueshifted ( $\approx -60$  km s $^{-1}$ ) emission apparently is observed, although the S/N is poor. Table 1 shows that

significantly higher radial velocities are observed in the optical than in  $H_2$  for all four condensations, with optical line wings extending normally to about twice as high negative velocities.

Entrainment seems to be the most probable explanation for these results.<sup>2</sup> In this case the lower velocity  $H_2$  gas would be located in the outer part of the shear layer (mixing layer) between the jet and the ambient  $H_2$ , where it has been accelerated only slightly. The material in the blue wings would be located near the inner part of the shear layer, i.e., closer to the flow axis. We note that entrainment of molecular material in the H I component of the HH 7–11 flow is also indicated by the 21 cm observations of Lizano *et al.* (1988).

The similar highly blueshifted velocity of the optical lines in HH 11 and the wing of the S(1) line (if real) is remarkable. Perhaps, near this object the entrained  $H_2$  is more efficiently accelerated. On the other hand, it is unclear why the optical radial velocities of HH 11 are so much higher than in the other condensations. This may result from the local orientation of the flow (e.g., deflection of the flow toward the line of sight) or from variations in the flow velocity (i.e., temporary enhancement).

Can any of the other cases of the jet model explain the data? A bow shock can be excluded since the  $H_2$  line is found all along the collimated flow and not merely at the end. (We note that Solf and Böhm 1987 encountered severe difficulties interpreting HH 7 as the working surface of a jet, which suggests that the flow terminates beyond HH 7 in a region with no optical emission.) The extreme case of entrained  $H_2$  moving at the full jet speed can also be excluded, since the observed radial velocities of the  $H_2$  are far too low. However, external shocks (case [2]) may be responsible for part of the  $H_2$  line emission in HH 7–11. They would mainly contribute to the emission near zero velocity with respect to the molecular cloud (i.e., at  $V_{\text{LSR}} = 7$  km s $^{-1}$ ).

The external shocks might also explain the presence of quiescent HCO $^+$  line emission at  $V_{\text{LSR}} = 7$  km s $^{-1}$  observed by Rudolph and Welch (1988). Such shocks (associated with the internal shocks in the HH objects) could cause the ambient molecular gas to be compressed above the critical density for HCO $^+$  excitation ( $\approx 10^5$  cm $^{-3}$ ). Rudolph and Welch (1988) did not consider the external shock model proposed here but offered an interpretation of their observation in terms of shocked cloudlets, because the HCO $^+$  was in general observed downstream of the HH objects. However, the shocked cloudlet model is inconsistent with the optical data, if the cloudlets are fully embedded in the collimated flow associated with HH 7–11. The HH 11 optical line profiles of Solf and Böhm (1987) show that the flow velocity is at least 250 km s $^{-1}$ . Therefore, if cloudlets are fully embedded in the flow, bow shocks with correspondingly high excitation should be observed around the individual cloudlets (HH objects). This is in contrast with the extremely low degree of excitation ( $v_{\text{shock}} \approx 40$  km s $^{-1}$ ) observed in these objects.

**HH 40.**—In the optical HH 40 is a bright knot *within* the HH 33/40 jet, i.e., it is *not* associated with the end of the flow, which is probably marked by HH 33 (Mundt, Brugel, and Bührke 1987). HH 40 and its associated jet are redshifted with typical radial velocities of about 100 km s $^{-1}$  in H $\alpha$  (Mundt, Brugel, and Bührke 1987). The shocked  $H_2$  is redshifted too:

<sup>2</sup> This confirms the suspicion of Liseau, Sandell, and Knee (1988) who proposed that the Kelvin-Helmholtz instability at the interface between the optical and the CO flows would produce clumps of dense molecular material within the jet flow from SSV 13.

the  $S(1)$  peak velocity is slightly redshifted with respect to CO and, more importantly, a broad red wing extends to about  $+80 \text{ km s}^{-1}$ . The  $S(1)$  profile is essentially the mirror image of those of HH 7–11. Therefore, entrainment of H<sub>2</sub> is also the most attractive model for the  $S(1)$  line emission in HH 40. However, as in HH 7–11, some of the low-velocity H<sub>2</sub> line emission may result from external shocks moving into the quiescent molecular gas.

*HH 19 and HH 43B.*—Either detailed H<sub>2</sub> maps or detailed high-resolution spectroscopic studies in the optical are lacking for both of these objects. Furthermore both objects show small radial velocities in H $\alpha$  and H<sub>2</sub>  $S(1)$ , and therefore these flows must be oriented close to the plane of the sky. This, as discussed above, makes the distinction between the proposed models rather difficult. In case of HH 43 it has been suggested by Schwartz, Dopita, and Cohen (1985) that the excitation structure in HH 43 can be explained by a cloudlet embedded in a collimated outflow (i.e., by a bow shock formed around that cloudlet). The relatively symmetric H<sub>2</sub> line profile of HH 43B is consistent with such an idea. However, symmetric profiles are also expected in the other cases discussed here, if the flow is oriented close to the plane of the sky.

*HH 32A.*—This HH object is associated with the T Tauri star AS 353A. HH 32A represents the brightest knot at the end of a redshifted jetlike feature extending from AS 353A. The outflow from the star is bipolar (Mundt, Stocke, and Stockman 1983). Recent optical imaging and high-resolution spectroscopic observations are discussed by Hartigan, Mundt, and Stocke (1986) and Solf, Böhm, and Raga (1986). Most of the observed  $S(1)$  line emission is associated with HH 32A (Zealey *et al.* 1986, 1988). It is remarkable that the  $S(1)$  line, like the optical lines, shows two components of which one is at very high radial velocity. The high-velocity components have very similar velocities ( $267$  and  $270 \text{ km s}^{-1}$ , see Table 1). However, the radial velocity of the lower velocity component is between  $30$ – $50 \text{ km s}^{-1}$  higher in the optical, depending on the particular optical line used for the comparison (e.g., H $\alpha$  or [S II]  $\lambda 6731$ ).

The two components in the optical line profiles of HH 32A have previously been explained by the following two models (Solf, Böhm, and Raga 1986, Hartigan, Mundt, and Stocke 1986).

*Model (a).*—A “pure” bow shock model, in which the bulk of the optical line emission originates in the radiative bow shock where both velocity components are formed. To explain the high radial velocities, bow shock velocities of about  $300 \text{ km s}^{-1}$  are required and the flow axis must be close to the line of sight (within  $\approx 20^\circ$ ). However, the application of this model to the  $S(1)$  line profile results in the following difficulty: because of the high bow shock velocities required, H<sub>2</sub> line emission can only form very far from the bow shock apex (that is, in those parts of the wings of the bow shock where the velocity components perpendicular to the shock surface are sufficiently small; i.e.,  $v_{\text{shock}} < 40 \text{ km s}^{-1}$ , see § I). Also H<sub>2</sub> probably cannot form at a significant rate in the cooling regions of the high-velocity shocks near the bow shock apex (see § IVb, above). Therefore, the range of H<sub>2</sub> velocities should be much smaller than in the optical lines. Roughly speaking, the bow shock wings act merely as a “heating agent” to the surrounding H<sub>2</sub> gas without accelerating it. Thus a “pure” bow shock model is only consistent with the lower velocity H<sub>2</sub> component, and not with the high-velocity component. This difficulty is not encountered in the jet model.

*Model (b).*—A jet model; in this model HH 32A is the jet’s

working surface (Hartigan, Mundt, and Stocke 1986). Only the low-velocity component originates in the bow shock of the working surface, since the working surface is propagating relatively slowly ( $\approx 80 \text{ km s}^{-1}$ ), as is indicated by the small tangential motion of HH 32A ( $\approx 50 \text{ km s}^{-1}$ ; Herbig and Jones 1983) and the small radial velocities of the low-velocity optical component ( $+67 \text{ km s}^{-1}$ , see Table 1). The high-velocity component is probably formed in oblique internal shocks before the jet’s end. If the H<sub>2</sub> components are explained in the same way as the optical components, the high-velocity H<sub>2</sub> is flowing with the full jet speed, whereas the low-velocity H<sub>2</sub> is external molecular gas heated in the bow shock (or perhaps decelerated jet material). The low-velocity component has a smaller radial velocity in H<sub>2</sub> than in H $\alpha$  ( $18 \text{ km s}^{-1}$  and  $67 \text{ km s}^{-1}$ , respectively). As outlined above, this is expected from bow shock theory, since the H<sub>2</sub> line emission is formed in the wings of the bow shock where the (external) H<sub>2</sub> will be accelerated far less than gas near the apex. As outlined in § IVb, the high-velocity H<sub>2</sub> could have been entrained close to the source. This model should be tested by spatially resolved  $S(1)$  line spectroscopy and deeper H<sub>2</sub> line imaging. For example, the  $S(1)$  line emission observed near HH 32D (i.e., closer to the source; see the map in Zealey *et al.* 1986, 1988) should show mainly high-velocity emission, as in the optical.

Thus we see that H<sub>2</sub> infrared data can be very helpful for testing models based on optical data. We conclude that the currently available data on HH 32A apparently favor the jet/H<sub>2</sub> entrainment model.

## V. CONCLUSIONS

We have argued that the following two mechanisms seem to be most important for explaining the observed H<sub>2</sub> 2.12  $\mu\text{m}$  line profiles of HH objects that are associated with collimated outflows:

1. Entrainment of external molecular gas, originally surrounding the jet, which is shock-heated by shocks in the jet itself or in its shear layer.
2. Shock-heating of the external H<sub>2</sub> gas in the wings of a bow shock associated with the working surface of a jet (this applies primarily to HH objects located at the ends of flows).

Mechanism (1), if correct, implies that the H<sub>2</sub> line emission may be used to study the direct interaction of collimated mass outflows with the ambient H<sub>2</sub>.

However, in several cases it cannot be excluded that H<sub>2</sub> surrounding a jet is heated by “external” shocks, i.e., low-velocity shocks moving into the external quiescent medium and being excited by the collimated flow. Since the H<sub>2</sub> excited in such a manner should have low velocities, the relevance of this mechanism can be tested only by higher resolution spectroscopy. Objects with high radial velocities should be employed for this test, because they give the best chance to detect velocity differences between the optical lines and the lines of shocked H<sub>2</sub>.

In the future, two-dimensional infrared detector arrays, such as IRCAM at UKIRT, when combined with Fabry-Perot spectrometers will allow detailed H<sub>2</sub> velocity mapping with spatial resolution of the order of  $1''$ . Such data will allow us to refine the simple models discussed here.

We wish to thank the staff of UKIRT for their support of these observations. It is a pleasure to acknowledge helpful comments by K. H. Böhm, M. Cameron, A. Raga, R. G. Smith, and P. M. Williams.

## REFERENCES

- Böhm, K. H., and Solf, J. 1985, *Ap. J.*, **294**, 533.  
 ———. 1989, in preparation.  
 Bührke, T., Mundt, R., and Ray, T. 1988, *Astr. Ap.*, **200**, 99.  
 Cantó, J., and Rodríguez, L. F. 1980, *Ap. J.*, **239**, 982.  
 Draine, B. T., Roberge, W. G., and Dalgarno, A. 1983, *Ap. J.*, **264**, 485.  
 Dyson, J. E. 1984, in *Gas in the Interstellar Medium*, ed. P. M. Ghondalekhar (Chilton: RAL Publications), p. 107.  
 Edwards, S., and Snell, R. L. 1983, *Ap. J.*, **270**, 605.  
 Elias, J. H. 1980, *Ap. J.*, **241**, 728.  
 Graham, J. A., and Elias, J. H. 1983, *Ap. J.*, **272**, 615.  
 Hartigan, P., Mundt, R., and Stocke, J. 1986, *A.J.*, **91**, 1357.  
 Hartigan, P., Raymond, J. C., and Hartmann, L. 1987, *Ap. J.*, **316**, 323.  
 Hartmann, L., and Raymond, J. C. 1984, *Ap. J.*, **276**, 560.  
 Hartquist, T. W., and Dyson, J. E. 1987, *M.N.R.A.S.*, **228**, 958.  
 Harvey, P. M., Joy, M., Lester, D. F., and Wilking, B. A. 1986, *Ap. J.*, **301**, 341.  
 Herbig, G. H., and Jones, B. F. 1981, *A.J.*, **86**, 1232.  
 ———. 1983, *A.J.*, **88**, 1040.  
 Hollenbach, D., and McKee, C. F. 1979, *Ap. J. Suppl.*, **41**, 555.  
 ———. 1980, *Ap. J. (Letters)*, **241**, L47.  
 Hollenbach, D. J., Werner, M. W., and Salpeter, E. E. 1971, *Ap. J.*, **163**, 165.  
 Lada, C. J. 1985, *Ann. Rev. Astr. Ap.*, **23**, 267.  
 Lane, A. P., and Bally, J. 1986, *Ap. J.*, **310**, 820.  
 Lightfoot, J. F., and Glencross, W. M. 1986, *M.N.R.A.S.*, **221**, 993.  
 Liseau, R., Sandell, G., and Knee, L. B. G. 1988, *Astr. Ap.*, **192**, 153.  
 Lizano, S., Heiles, C., Rodríguez, L. F., Koo, B.-C., Shu, F. H., Hasegawa, T., Hayashi, S., and Mirabel, I. F. 1988, *Ap. J.*, **328**, 763.  
 Meaburn, J., and Dyson, J. E. 1987, *M.N.R.A.S.*, **225**, 863.  
 Mundt, R. 1985a, *Lecture Notes in Physics*, Vol. **217**, *Nearby Molecular Clouds*, ed. G. Serra (Heidelberg: Springer), p. 160.  
 ———. 1985b, in *Protostars and Planets II*, ed. D. Black and M. Matthews (Tucson: University of Arizona Press), p. 414.  
 ———. 1986, *Canadian J. Phys.*, **64**, 407.  
 ———. 1987, in *Circumstellar Matter*, ed. I. Appenzeller and C. Jordan (Dordrecht: Reidel), p. 147.  
 ———. 1988, in *Formation and Evolution of Low Mass Stars* (NATO Advanced Study Institute), ed. A. K. Dupree and M. T. V. T. Lago (Dordrecht: Kluwer), p. 257.  
 Mundt, R., Brugel, E. W., and Bührke, T. 1987, *Ap. J.*, **319**, 275.  
 Mundt, R., Bührke, T., Fried, J. W., Neckel, T., Sarcander, M., and Stocke, J. 1984, *Astr. Ap.*, **140**, 17.  
 Mundt, R., and Fried, J. W. 1983, *Ap. J. (Letters)*, **274**, L83.  
 Mundt, R., Stocke, J., and Stockman, H. S. 1983, *Ap. J. (Letters)*, **265**, L71.  
 Nadeau, D., and Geballe, T. R. 1979, *Ap. J. (Letters)*, **230**, L169.  
 Norman, C. A., and Silk, J. 1979, *Ap. J.*, **228**, 197.  
 Norman, M. L., Smarr, L., and Winkler, K.-H. 1984, in *Numerical Astrophysics, Festschrift in Honor of James R. Wilson*, ed. J. Cantrella, J. LeBlanc, and R. Bowers (Boston: Jones & Bartlett), p. 88.  
 Raga, A. C. 1986, *A.J.*, **92**, 637.  
 Raga, A. C., and Böhm, K.-H. 1986, *Ap. J.*, **308**, 829.  
 ———. 1987, *Ap. J.*, **323**, 193.  
 Raga, A. C., Mateo, M., Böhm, K. H., and Solf, J. 1988, *A.J.*, **95**, 1783.  
 Reipurth, B., Bally, J., Graham, J. A., Lane, A. P., and Zealey, W. J. 1986, *Astr. Ap.*, **164**, 51.  
 Rudolph, A., and Welch, W. J. 1988, *Ap. J. (Letters)*, **326**, L31.  
 Sandell, G., Zealey, W. J., Williams, P. M., Taylor, K. N. R., and Storey, J. V. 1987, *Astr. Ap.*, **182**, 237.  
 Schwartz, R. D. 1983, *Ann. Rev. Astr. Ap.*, **21**, 209.  
 Schwartz, R. D., Cohen, M., and Williams, P. M. 1987, *Ap. J.*, **322**, 403.  
 Schwartz, R. D., and Dopita, M. A. 1980, *Ap. J.*, **236**, 543.  
 Schwartz, R. D., Dopita, M. A., and Cohen, M. 1985, *A.J.*, **90**, 1820.  
 Shull, J. M., and Hollenbach, D. J. 1978, *Ap. J.*, **220**, 525.  
 Solf, J. 1987, *Astr. Ap.*, **184**, 322.  
 Solf, J., and Böhm, K. H. 1987, *A.J.*, **93**, 1172.  
 Solf, J., Böhm, K. H., and Raga, A. C. 1986, *Ap. J.*, **305**, 795.  
 Strom, K. M., Strom, S. E., Wolff, S. C., Morgan, J., and Wentz, M. 1986, *Ap. J. Suppl.*, **62**, 39.  
 Strom, S. E., Strom, K. M., Grasdalen, G. L., Sellgren, K., Wolff, S., Morgan, J., Stocke, J., and Mundt, R. 1985, *A.J.*, **90**, 2281.  
 Zealey, W. J., Williams, P. M., Geballe, T. R., Sandell, G., Zinnecker, H., Mundt, R., and Taylor, K. 1988, *Vistas Astr.*, **31**, 479.  
 Zealey, W. J., Williams, P. M., and Sandell, G. 1984, *Astr. Ap.*, **140**, L31.  
 Zealey, W. J., Williams, P. M., Taylor, K., Storey, J., and Sandell, G. 1986, *Astr. Ap.*, **158**, L9.  
 Zealey, W. J., et al. 1989, in preparation.  
 Zinnecker, H., Mundt, R., Williams, P. M., and Zealey, W. J. 1985, *Mitt. Astr. Ges.*, **63**, 234.

T. R. GEBALLE: Joint Astronomy Centre, 665 Komohana Street, Hilo, HI 96720

REINHARD MUNDT: Max-Planck-Institut für Astronomie, Königstuhl, D-6900 Heidelberg, Federal Republic of Germany

WILLIAM J. ZEALEY, Physics Department, University of Wollongong, P.O. Box 1144, N.S.W. 2500, Australia

HANS ZINNECKER: Max-Planck-Institut für Physik und Astrophysik, Institut für Extraterrestrische Physik, Karl-Schwarzschild-Strasse 1, D-8046 Garching, Federal Republic of Germany